Unbalanced Radial Current Flow Simulation of No-Insulation REBCO Pancake Coils During Normal State Transition

Thomas Kurauchi[1] and So Noguchi[1]

[1] Graduate School of Information Science and Technology, Hokkaido University, Sapporo 060-0814, Japan

E-mail: kurauchi@em.ist.hokudai.ac.jp

Received xxxxxx
Accepted for publication xxxxxx
Published xxxxxx

Abstract

The no-insulation (NI) winding technique greatly enhances the thermal stability of REBCO ($REBa_2Cu_3O_x$, RE = Rare Earth) pancake coils by avoiding burning-out and thermal runaway. The complicated electrical behaviors in NI REBCO pancake coils produce the convoluted mechanical behaviors, so that some journal papers reported that high-field NI REBCO pancake coils were mechanically damaged during quench. To apply NI REBCO magnets to practical commercial use, it is important to understand the electromagnetic and mechanical behaviors of NI REBCO pancake coils in detail by both experiments and simulations. To clarify the electrical behaviors, a few simulation methods for NI REBCO pancake coils have been proposed; such as a simple RL parallel equivalent circuit. In these previous models, the radial current paths along the top and bottom of pancake coils are represented as one current circuit path. Actually, since the radial current path of the bottom of one pancake coil is very close to that of the top of the next lower coil, the inductive behavior between these two paths appears. The simulation results show a probability that the different amount of radial currents on the top and bottom of one pancake coil are carried during quench.

Keywords: No-insulation REBCO pancake coils, normal state transition, parallel equivalent circuit model

1. Introduction

In these days, it is strongly desired to apply 2nd-generation high temperature superconducting (HTS) magnets to practical applications, which need strong magnetic field, such as magnetic resonance imaging (MRI) [1,2], nuclear magnetic resonance (NMR) [3,4], and particle accelerators [5,6]. A no-insulation (NI) winding technique [7,8,9] is raising attention in developing these applications, because it greatly improves the thermal stability of $REBa_2Cu_3O_x$ (REBCO, RE = Rare Earth) magnets by avoiding burning-out and thermal runaway. Recently, a REBCO insert magnet successfully generated a world record 45.5-T DC magnetic field using the NI winding technique [10]. Although the quench of NI REBCO pancake coils occurred, the burning-out was avoided. Meanwhile, the induced currents or the screening currents caused a plastic deformation to REBCO tapes [10,11]. As another example, the NI REBCO insert magnet of the MIT 1.3-GHz NMR had complicated mechanical damages during normal state transition in a standalone test [12,13]. Toward practical commercial use of NI REBCO magnets, it is important to grasp the electromagnetic behaviors of NI REBCO pancake coils in detail by both experiments and simulations. The convoluted current behaviors result in various mechanical forces/stresses; *i.e.*, hoop stress/strain, axial force, torque, and

REBCO tape plastic deformation [14]. Based on such backgrounds, the importance of obtaining the detailed current phenomenon is increasing, *e.g.*, the current distribution in NI REBCO pancake coil [15,16], the screening current in REBCO tapes [17,18].

In our previous research using a partial element equivalent circuit model (PEEC), a torque simulation on NI REBCO double pancake coil have been conducted [19]. When a normal state transition occurred in an NI REBCO pancake coil, the operating current changed from the circumferential to the radial direction through the contact of turns. A Lorentz force was generated due to the radial currents and the axial magnetic field. This force appeared as a torque in REBCO coils. The possibility of damaging terminals or coils themselves during quench have been shown in the previous paper [19].

As a simulation of NI REBCO pancake coil, a simple parallel equivalent circuit (called "SPEC" in this paper) model firstly appeared in [7], and the details of the model were described in [11]. In this paper, to investigate the detail of the radial currents, we propose a modified simple parallel equivalent circuit (mSPEC) model. The unbalanced radial currents on the top and bottom of pancake coils are simulated and discussed.

2. Simulation of normal state transition characteristic of NI REBCO double pancake coil

A. mSPEC model for unbalanced radial currents

When a normal state transition happens in an NI REBCO pancake coil, the circumferential current starts flowing into the radial path from turn to turn. Figure 1 shows a cross-sectional view of NI REBCO pancake coils, where I_θ is the circumferential current, and I_{tp} and I_{bt} are the radial ones along the top and bottom of pancake coils, respectively. The radial current path through the turn-to-turn contact is divided to the top and bottom radial current paths I_{tp} and I_{bt} due to a high resistance of Hastelloy, as shown in Figure 1. The top and bottom radial currents, I_{tp} and I_{bt}, have resistive and inductive characteristics, separately.

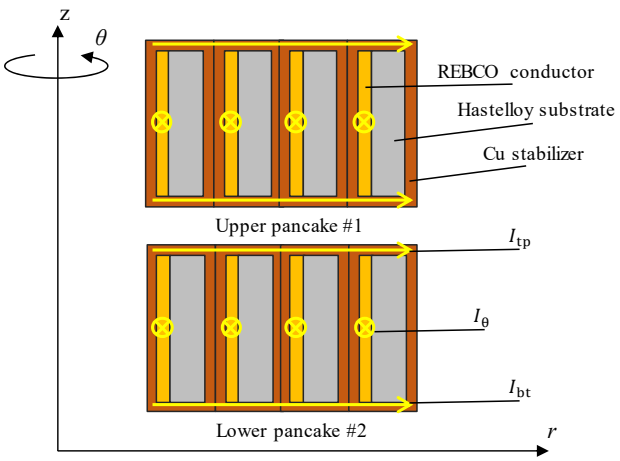

Figure 1. The radial bypassing currents I_{tp} and I_{bt} flow through the copper stabilizers along the top and bottom of pancake coils.

The ordinary SPEC model shown in Figure 2 has been widely used to simulate the current behavior of NI REBCO pancake coils [7,9,11]. Here, I_θ, I_r, I_{st}, and I_{re} are, respectively, the azimuthal current, the radial current, the copper stabilizer current, and the REBCO layer current. R_c, R_{st}, and R_{re} are the resistances of turn-to-turn contact, copper stabilizer, and REBCO layer, respectively. L_θ and M_θ are the self- and mutual-inductances. As shown in Figure 2, by neglecting the inductive components of radial current paths in the ordinary SPEC model, the top and bottom radial current paths are combined as one radial current path with only the turn-to-turn contact resistance R_c.

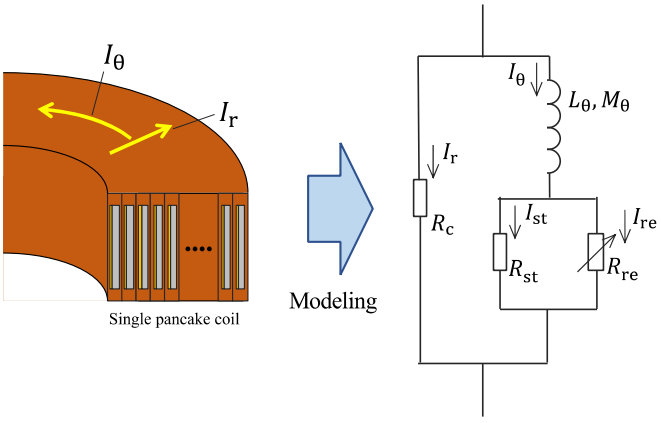

Figure 2. Ordinary simple parallel equivalent circuit (SPEC) model [7,11] consisting of RL parallel circuit. The radial current path is represented by only one contact resistance R_c.

Meanwhile, the journal paper [20] clarified that the exact turn-to-turn contact resistance R_c was presented as follows:

$$R_c = \frac{R'_{Cu} R_{Has}}{R'_{Cu} + R_{Has}} + R_{ct} \quad (1)$$

where R'_{Cu}, R_{Has}, and R_{ct} are the resistances of radial copper stabilizer, Hastelloy substrate, and the actual turn-to-turn contact resistance, respectively, (see Figure 3). Since $R'_{\mathrm{Cu}} \ll R_{\mathrm{ct}}$ and $R_{\mathrm{Has}} \gg R_{\mathrm{ct}}$, the combined resistance R_{c} is almost equal to the actual turn-to-turn contact resistance R_{ct}:

$$R_{\mathrm{c}} = \frac{R'_{\mathrm{Cu}} R_{\mathrm{Has}}}{R'_{\mathrm{Cu}} + R_{\mathrm{Has}}} + R_{\mathrm{ct}} \approx R_{\mathrm{ct}} \tag{2}$$

In the ordinary SPEC model, eventually, the radial resistive component is represented as R_{c} by ignoring the resistive and inductive characteristics of the radial current paths, I_{tp} and I_{bt}.

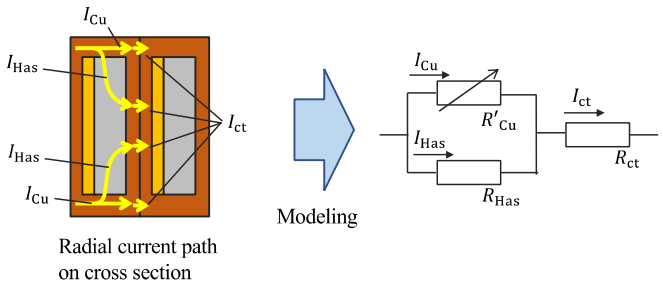

Figure 3. Detailed equivalent circuit of radial connection of REBCO tapes in NI REBCO coil [20]. R_{ct}, R'_{Cu}, and R_{Has} are the resistances of actual turn-to-turn contact, radial copper stabilizer, and Hastelloy substrate, respectively. The contact resistance R_{c} in Figure 2 is a resistance combined with R_{ct}, R'_{Cu}, and R_{Has}.

To model an actual radial current path, we propose a new equivalent circuit model, as shown in Figure 4, where L_{tp}, M_{tp}, L_{bt}, and M_{bt} are the self- and mutual-inductances of the top and bottom radial current paths, respectively. R_{Cu} is the resistance of copper stabilizer on radial current path, and R_{ct} is the actual turn-to-turn contact resistance. Since the Hastelloy substrate is regarded as insulation, the radial bypassing currents I_{tp} and I_{bt} flow through the edges of copper stabilizer, *i.e.*, along the top and bottom of pancake coil, as shown in Figure 1. When the radial current path along the bottom of one pancake coil is very close to that along the top of the next lower coil, the inductive behavior between these two paths must be considered. Meanwhile, the actual turn-to-turn contact path can be expressed as one current path according to Figure 3 [20]. In the mSPEC model, the inductive and resistive components of the radial current paths I_{tp} and I_{bt} through the copper stabilizer are newly taken into account, in spite of ignoring them in the ordinary SPEC model. When the resistive voltages on R_{Cu} are lower than the inductive voltages of L_{bt}, M_{bt}, L_{tp}, and M_{tp}, the unbalanced current would be induced according to the difference of the top and bottom inductive voltages.

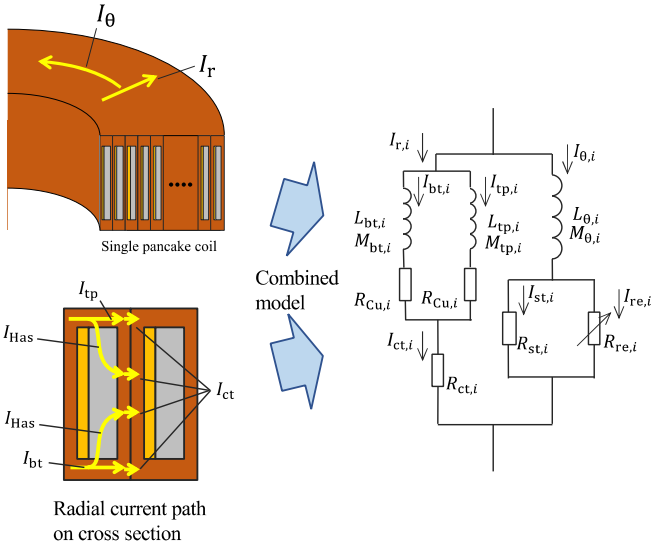

Figure 4. mSPEC model is a combined model of the ordinary SPEC model in Figure 2 and the actual radial contact model in Figure 3. The radial current path I_{Cu} in Figure 3 is separated to I_{tp} and I_{bt}, which individually have the parallel inductive and resistive components. The Hastelloy resistance are neglected due to its large value.

B. Normal state transition simulation

To simulate the newly proposed mSPEC model, the following equations are numerically solved:

$$I_{\mathrm{tp},i} + I_{\mathrm{bt},i} + I_{\mathrm{st},i} + I_{\mathrm{re},i} = I_{\mathrm{op}} \tag{3}$$

$$V_{L_{\mathrm{tp}},i} + R_{\mathrm{Cu},i} I_{\mathrm{tp},i} = V_{L_{\mathrm{bt}},i} + R_{\mathrm{Cu},i} I_{\mathrm{bt},i} \tag{4}$$

$$R_{\mathrm{st},i} I_{\mathrm{st},i} = R_{\mathrm{re},i} I_{\mathrm{re},i} \tag{5}$$

$$V_{L_{\theta,}i} + R_{\mathrm{st},i} I_{\mathrm{st},i} = V_{L_{\mathrm{bt}},i} + R_{\mathrm{Cu},i} I_{\mathrm{bt},i} + R_{\mathrm{ct},i}\left(I_{\mathrm{tp},i} + I_{\mathrm{bt},i}\right) \tag{6}$$

$$R_{\mathrm{re},i} = \frac{E_{\mathrm{c}} l_i}{I_{\mathrm{c},i}} \left| \frac{I_{\mathrm{re},i}}{I_{\mathrm{c},i}} \right|^{n-1} \tag{7}$$

where i, I_{op}, $V_{L_{\mathrm{tp}},i}$, $V_{L_{\mathrm{bt}},i}$, $V_{L_{\theta,}i}$, E_{c}, l_i, $I_{\mathrm{c},i}$, and n are the coil number, the operating current, the top and bottom radial inductance voltages, the circumferential inductance voltage, the electrical field criterion at critical current (1 μV/cm in this paper), the tape length of coil, the critical current, and the power index value, respectively.

The coil specifications and the simulation conditions are summarized in Tables 1 and 2, respectively. In this simulation, the contact resistivity ρ_{c} is supposed to be 70 $\mu\Omega \cdot \mathrm{cm}^2$ [9] to calculate R_{ct}. The critical current I_{c} is given as a function of the magnetic field and its orientation to the wide surface of REBCO tapes. The used approximation equations on the critical current are obtained from experiments [21]. All the

self- and mutual-inductances are calculated from derivation given in [11].

Table 1. Tape and coil specifications

Parameters	Units	Values
REBCO tape		
Tape width	[mm]	6.0
Tape thickness	[μm]	100
Cu stabilizer thickness	[μm]	20
REBCO layer thickness	[μm]	1.0
I_c @ 77 K, self field	[A]	180
n-value	[-]	30
Double pancake coil		
Coil i.d.; o.d.	[mm]	100; 120
Coil height per single pancake	[mm]	6.0
Distance between pancake coils	[mm]	1.0
Number of turns per pancake	[turn]	100
Contact resistivity	[μΩcm^2]	70
R_c (each single pancake coil)	[μΩ]	339
Total coil inductance	[mH]	6.4

Table 2. Simulation conditions

Parameters	Units	Values
Simulation time step	[ms]	0.01
Quench time	[ms]	1.0
Temperature	[K]	4.2, 77.0
Operating current	[A]	60.0

In the simulation, the quench events were modeled by manually increasing the REBCO resistance R_{re} to an extremely high value. To solve the nonlinear equations (3)-(7) caused by the n-value model, the Newton-Raphson method is adopted for numerical computation.

When a normal state transition occurs in the upper coil, the current flow changes into the radial direction through the contact surface of the REBCO tapes. As shown in the previous simulation results [11], the radial current in the lower coil is induced in the same direction as the upper coil to compensate the magnetic field of the normal-state-transitioned upper coil.

3. Simulation results

In the quench simulation, the upper coil is quenched at 1 ms when a DC transport current of 60 A carries. The current behavior in the REBCO layer, Cu stabilizer, and the top and bottom radial currents are investigated.

Table 3 shows the inductances M_r of the radial current paths in matrix form. As can be seen in Table 3, these inductances are small. When the inductances M_r are much smaller than the radial Cu stabilizer resistance R_{Cu}, R_{Cu} dominates in the radial current behavior. Meanwhile, when M_r is close to or higher than R_{Cu}, the inductive behavior is observed. Therefore, two simulations were conducted with the different radial Cu stabilizer resistances $R_{Cu} = 2.89$ μΩ (at 77 K) and 28.9 nΩ (at 4.2 K).

Table 3. Inductance matrix

M_r [nH]	tp_1	bt_1	tp_2	bt_2
tp_1	0.133	0.114	-0.110	-0.086
bt_1	0.114	0.133	-0.132	-0.110
tp_2	-0.110	0.132	0.133	0.114
bt_2	-0.086	-0.110	0.114	0.133

A. *Simulation at 77 K*

Figures 5 and 6 plot the time-varying currents of the upper and lower pancake coils, respectively. The REBCO layer current on the upper coil goes to 0 immediately after quench at 1 ms, and the radial currents on the top and bottom of the upper pancake coil gradually decrease (here, the positive means the radially outward direction). On the lower coil, the REBCO layer current increases due to the compensation of losing the magnetic field of the upper coil, and the top and bottom of the lower pancake coil gradually decrease, too. On both the upper and lower coils, the radial currents are balanced on the top and bottom of the pancake coils. That is, the radial Cu stabilizer resistance R_{Cu} are enough large.

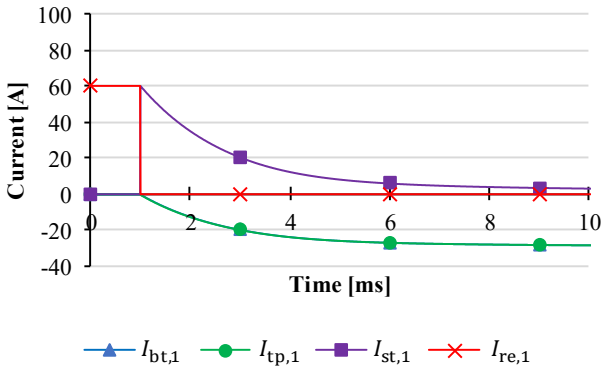

Figure 5. Current behaviors of upper coil after normal state transition happened with Cu stabilizer resistance $R_{Cu} = 2.89$ μΩ at 77 K.

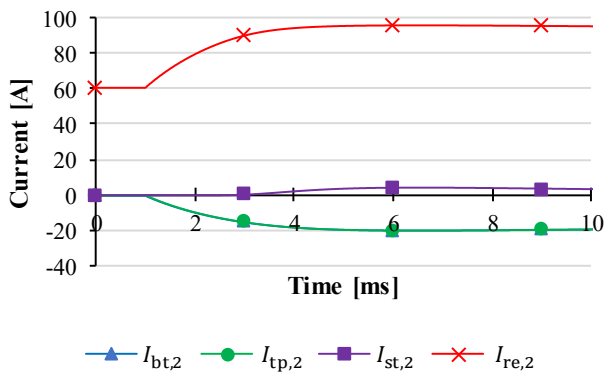

Figure 6. Current behaviors of lower coil after normal state transition happened with Cu stabilizer resistance $R_{Cu} = 2.89$ μΩ at 77 K.

Figure 7 shows the torque curve as the function of time. No difference of torque on the top and bottom of each pancake coil can be seen. The torques on the lower coil are larger than those on the upper one. Whereas, the magnitude of torques are very small, because small magnetic field is generated by one double pancake.

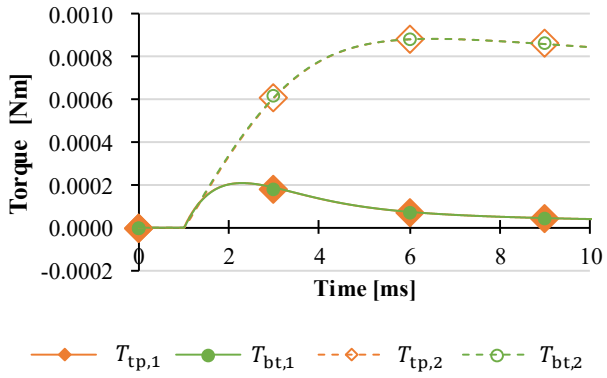

Figure 7. Torque behaviors of upper and lower coils after normal state transition happened with Cu stabilizer resistance $R_{Cu} = 2.89$ μΩ at 77 K. The positive means the counterclockwise direction.

For comparison of the ordinary and the modified SPEC model, Figures 8 and 9 show the current behaviors of the upper and lower coils simulated by the ordinary SPEC model. As seen in Figures 5, 6, 8, and 9, the currents of the REBCO layer and copper stabilizer well agree between the ordinary and the modified SPEC. The total of radial top and bottom currents on Figures 5 and 6 are almost the same as the radial current on Figures 8 and 9. As a consequence, the mSPEC model corresponds to the ordinary SPEC when the copper stabilizer resistance R_{Cu} is large.

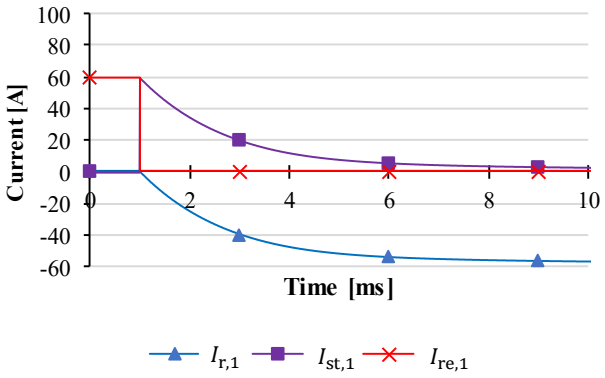

Figure 8. Current behaviors of upper coil after normal state transition happened with Cu stabilizer resistance $R_{Cu} = 2.89$ μΩ at 77 K, simulated with the ordinary SPEC model.

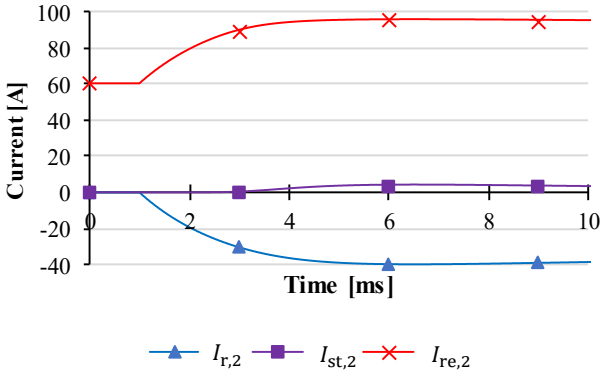

Figure 9. Current behaviors of lower coil after normal state transition happened with Cu stabilizer resistance $R_{Cu} = 2.89$ μΩ at 77 K, simulated with the ordinary SPEC model.

B. Simulation at 4.2 K

The copper stabilizer resistivity at 4.2 K is approximately 1/100 of that at 77 K. It is supposed that the radial inductive components including mutual inductances do not change with temperature. When the inductive voltages are much higher than the resistive voltage (*i.e.*, $V_{L_{tp}} \gg R_{Cu} I_{tp}$ and $V_{L_{bt}} \gg R_{Cu} I_{bt}$), the unbalanced currents, I_{tp} and I_{bt}, are induced by the difference of the inductive voltages on the top and bottom.

Figures 10 and 11 present the transient currents on the REBCO layer, Cu stabilizer, and the top and bottom radial paths. The different radial currents can be seen on the top and

bottom radial current on each pancake coil. After 6 ms, both the top and bottom radial currents converge to the same value.

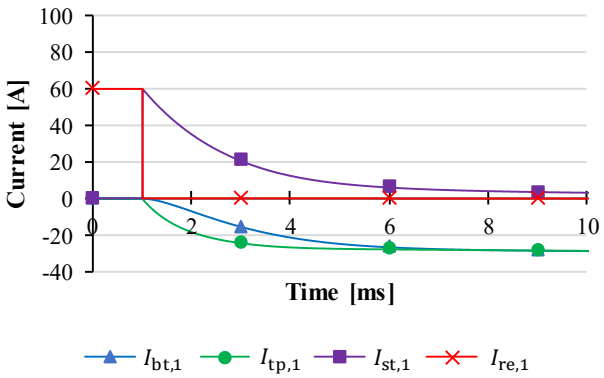

Figure 10. Current behaviors of upper coil after normal state transition happened with Cu stabilizer resistance $R_{Cu} = 28.9$ nΩ at 4.2 K.

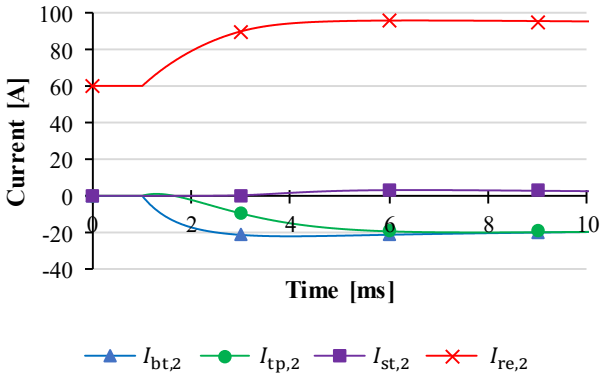

Figure 11. Current behaviors of lower coil after normal state transition happened with Cu stabilizer resistance $R_{Cu} = 28.9$ nΩ at 4.2 K.

Figure 12 shows the torques acting to the top and bottom of the upper and lower pancake coils. Since the unbalanced radial currents are induced, the different torques are generated on the top and bottom of each pancake coil. The clockwise torque appears on the top of the lower coil in spite of the counterclockwise torque on the bottom of the lower. That is, a twist force acts for the lower coil. As the magnetic field generated by 1 double pancake coil is very small, the torque difference is also small.

In spite of the high critical current at 4.2 K, the operating current is 60 A in simulation of 4.2 K in order to compare with the results of 77 K. When the higher current is carried, the larger torque is generated.

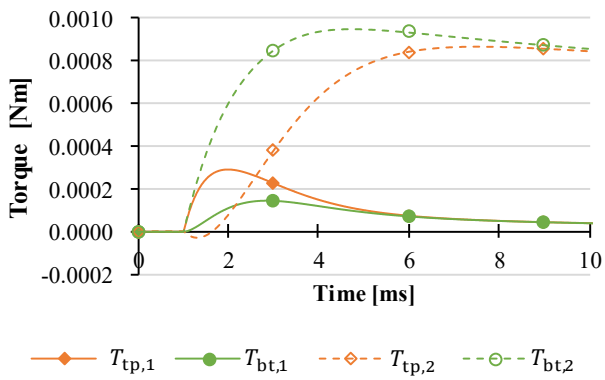

Figure 12. Torque behaviors of coils after normal state transition happened with Cu stabilizer resistance $R_{Cu} = 28.9$ nΩ at 4.2 K. The positive means the counterclockwise direction.

Our simulation shows the probability that an unbalanced torque occurs during normal-state transition when the radial inductive voltage is larger than the radial resistive one, but not confirmed by an experiment. The unbalanced torque is caused by the low resistance of copper stabilizer in the simulation. Therefore, the specifications of stabilizer, such as resistivity and thickness, are a key to avoid unbalanced torque. Whereas, when NI REBCO pancake coils are stacked for high magnetic field generation, there is, also, a possibility that a large unbalanced torque gives the coils mechanical damage. Hence, in the near future, it is necessary to simulate the torque behaviors of multi-stacked NI REBCO pancake coils, especially for use as an insert magnet.

4. Conclusion

The no-insulation (NI) winding technique greatly increases the thermal stability of REBCO pancake coils. As a next step, a high mechanical stability is required to practical applications, so that the detailed current must be clarified. To investigate the influence of the inductive components on the radial currents of NI REBCO pancake coils during quench, we have proposed a modified simple parallel equivalent circuit (mSPEC). From the simulation results, when the stabilizer resistance is enough low, unbalanced torques appear on the top and bottom of pancake coil.

In this paper, we showed a probability of unbalanced torque. Although the simulated torques are small due to a low magnetic field in this paper, a further investigation is needed under the condition of a high magnetic field. Also, a finer simulation model will be also required. However, previously proposed finer models [15,16] are too complicated to consider the actual radial current paths, and they need a large computer memory and a long computation time. Firstly, we will

simulate the radial currents and torques of multi-stacked NI REBCO pancake coils to generate an ultra high magnetic field using the mSPEC model, and then we will conduct an experiment to measure a twist torque in the near future.

References

[1] Miyazaki H, Iwai S, Otani Y, Takahashi M, Tosaka T, Tasaki K, Nomura S, Kurusu T, Ueda H, Noguchi S, Ishiyama A, Urayama S and Fukuyama H 2016 Design of a conduction-cooled 9.4 T REBCO magnet for whole-body MRI systems *Supercond. Sci. Technol.* **29** 104001

[2] Yokoyama S, Lee J, Imura T, Matsuda T, Eguchi R, Inoue T, Nagahiro T, Tanabe H, Sato S, Daikoku A, Nakamura T, Shirai Y, Miyagi D and Tsuda M 2017 Research and Development of the High Stable Magnetic Field ReBCO Coil System Fundamental Technology for MRI *IEEE Trans. Appl. Supercond.* **27** 4400604

[3] Iwasa Y, Bascuñán J, Hahn S, Voccio J, Kim Y, Lécrevisse T, Song J and Kajikawa K 2015 A high-resolution 1.3-GHz/54-mm LTS/HTS NMR magnet *IEEE Trans. Appl. Supercond.* **25** 4301205

[4] Maeda H and Yanagisawa Y 2019 Future prospects for NMR magnets: A perspective *Journal of Magnetic Resonance* **306** 80-85

[5] Ueda H, Fukuda M, Hatanaka K, Wang T, Wang X, Ishiyama A, Noguchi S, Nagaya S, Kashima N and Miyahara N 2013 Conceptual design of next generation HTS cyclotron *IEEE Trans. Appl. Supercond.* **23** 4100205

[6] Takayama S, Iwai S, Kubo Y, Koyanagi K, Miyazaki H, Orikasa T, Ishii Y, Kurusu T, Amemiya N, Ogitsu T, Iwata Y, Nod K and Yoshimoto M 2019 Development of an HTS Accelerator Magnet With REBCO Coils for Tests at HIMAC Beam Line *IEEE Trans. Appl. Supercond.* **29** 4004205

[7] Hahn S, Park D K, Bascuñán J and Iwasa Y 2011 HTS pancake coils without turn-to-turn insulation *IEEE Trans. Appl. Supercond.* **21** 1592

[8] Kim S B, Kaneko T, Kajikawa H, Joo J H, Jo J M, Han Y J and Jeong H S 2013 The transient stability of HTS coils with and without the insulation and with the insulation being replaced by brass tape *IEEE Trans. Appl. Supercond.* **23** 7100204

[9] Wang X, Hahn S, Kim Y, Bascuñán J, Voccio J, Lee H and Iwasa Y 2013 Turn-to-turn contact characteristics for an equivalent circuit model of no-insulation ReBCO pancake coil *Supercond. Sci. Technol.* **26** 035012

[10] Hahn S, Kim K, Kim K, Hu X, Painter T, Dixon I, Kim S, Bhattarai K R, Noguchi S, Jaroszynski J and Larbalestier D C 2019 45.5-tesla direct-current magnetic field generated with a high-temperature superconducting magnet *Nature* **570** 496–9

[11] Noguchi S 2019 Electromagnetic, Thermal, and Mechanical Quench Simulation of NI REBCO Pancake Coils for High Magnetic Field Generation *IEEE Trans. Appl. Supercond.* **29** 4602607

[12] Noguchi S, Park D, Choi Y, Lee J, Li Y, Michael P C, Bascuñán J, Hahn S and Iwasa Y 2019 Quench Analyses of the MIT 1.3-GHz LTS/HTS NMR Magnet *IEEE Trans. Appl. Supercond.* **29** 4301005

[13] Michael P C, Park D, Choi Y H, Lee J, Li Y, Bascuñán J, Noguchi S, Hahn S and Iwasa Y 2019 Assembly and Test of a 3-Nested-Coil 800-MHz REBCO Insert (H800) for the MIT 1.3 GHz LTS/HTS NMR Magnet *IEEE Trans. Appl. Supercond.* **29** 4300706

[14] Hahn S, Kim K L, Kim K, Bhattarai K, Radcliff K, Hu X, Painter T, Dixon I and Larbalestier D 2018 Progress in No-Insulation HTS Magnet Researches *presented at Applied Superconductivity Conference 2018*

[15] Wang T, Noguchi S, Wang X, Arakawa I, Minami K, Monma K, Ishiyama A, Hahn S and Iwasa Y 2015 Analyses of Transient Behaviors of No-Insulation REBCO Pancake Coils During Sudden Discharging and Overcurrent *IEEE Trans. Appl. Supercond.* **25** 4603409

[16] Markiewicz W D, Jaroszynski J, Abraimov D V, Joyner R E and Khan A 2016 Quench analysis of pancake wound REBCO coils with low resistance between turns *Supercond. Sci. Technol.* **29** 025001

[17] Ueda H, Fukuda M, Hatanaka K, Michitsuji K, Karino H, o Wang T, Wang X, Ishiyama A, Noguchi S, Yanagisawa Y and Maeda H 2014 Measurement and simulation of magnetic field generated by screening currents in HTS coil *IEEE Trans. Appl. Supercond.* **24** 4701505

[18] Noguchi S, Hahn S, Ueda H, Kim S B and Ishiyama A 2018 An Extended Thin Approximation Method to Simulate Screening Current Induced in REBCO Coils *IEEE Trans. Appl. Supercond.* **54** 7201904

[19] Noguchi S and Hahn S 2019 Torque Simulation on NI REBCO Pancake Coils during Quench *Journal of Physics: Conference Series* **1293** 012061

[20] Noguchi S, Monma K, Igarashi H and Ishiyama A 2016 Investigation of Current Flow between Turns of NI REBCO Pancake Coil by 2-D Finite-Element Method *IEEE Trans. Appl. Supercond.* **26** 4901205

[21] Ueda H, Imaichi Y, Wang T, Ishiyama A, Noguchi S, Iwai S, Miyazaki H, Tosaka T, Nomura S, Kurusu T, Urayama S and Fukuyama H 2016 Numerical Simulation on Magnetic Field Generated by Screening Current in 10-T-Class REBCO Coil *IEEE Trans. Appl. Supercond.* **26** 4701205